

MICM: Rethinking Unsupervised Pretraining for Enhanced Few-shot Learning

Zhenyu Zhang*

School of Computer Science and Technology, Huazhong University of Science and Technology
Wuhan, China
m202273680@hust.edu.cn

Guangyao Chen*

National Key Laboratory for Multimedia Information Processing, School of Computer Science, Peking University
Beijing, China
gy.chen@pku.edu.cn

Yixiong Zou[†]

School of Computer Science and Technology, Huazhong University of Science and Technology
Wuhan, China
yixiongz@hust.edu.cn

Zhimeng Huang

National Engineering Research Center of Visual Technology, School of Computer Science, Peking University
Beijing, China
zmhuang@pku.edu.cn

Yuhua Li[†]

School of Computer Science and Technology, Huazhong University of Science and Technology
Wuhan, China
idcliyuhua@hust.edu.cn

Ruixuan Li

School of Computer Science and Technology, Huazhong University of Science and Technology
Wuhan, China
rxli@hust.edu.cn

ABSTRACT

Humans exhibit a remarkable ability to learn quickly from a limited number of labeled samples, a capability that starkly contrasts with that of current machine learning systems. Unsupervised Few-Shot Learning (U-FSL) seeks to bridge this divide by reducing reliance on annotated datasets during initial training phases. In this work, we first quantitatively assess the impacts of Masked Image Modeling (MIM) and Contrastive Learning (CL) on few-shot learning tasks. Our findings highlight the respective limitations of MIM and CL in terms of discriminative and generalization abilities, which contribute to their underperformance in U-FSL contexts. To address these trade-offs between generalization and discriminability in unsupervised pretraining, we introduce a novel paradigm named Masked Image Contrastive Modeling (MICM). MICM creatively combines the targeted object learning strength of CL with the generalized visual feature learning capability of MIM, significantly enhancing its efficacy in downstream few-shot learning inference. Extensive experimental analyses confirm the advantages of MICM, demonstrating significant improvements in both generalization and discrimination capabilities for few-shot learning. Our comprehensive quantitative evaluations further substantiate the superiority of MICM, showing that our two-stage U-FSL framework based on MICM markedly outperforms existing leading baselines. The repository of this project is available at <https://github.com/iCGY96/MICM>.

*Equal Contribution.

[†]Corresponding authors.

Permission to make digital or hard copies of all or part of this work for personal or classroom use is granted without fee provided that copies are not made or distributed for profit or commercial advantage and that copies bear this notice and the full citation on the first page. Copyrights for components of this work owned by others than the author(s) must be honored. Abstracting with credit is permitted. To copy otherwise, or republish, to post on servers or to redistribute to lists, requires prior specific permission and/or a fee. Request permissions from permissions@acm.org.

ACM MM, 2024, Melbourne, Australia

© 2024 Copyright held by the owner/author(s). Publication rights licensed to ACM.

ACM ISBN 978-1-4503-XXXX-X/18/06

<https://doi.org/10.1145/3664647.3680647>

CCS CONCEPTS

• **Computing methodologies** → **Computer vision**.

KEYWORDS

Unsupervised Few-shot Learning, Contrastive Learning, Masked Image Modeling, Masked Image Contrastive Modeling

ACM Reference Format:

Zhenyu Zhang, Guangyao Chen*, Yixiong Zou, Zhimeng Huang, Yuhua Li[†], and Ruixuan Li. 2024. MICM: Rethinking Unsupervised Pretraining for Enhanced Few-shot Learning. In *Proceedings of the 32nd ACM International Conference on Multimedia (MM'24)*, October 28–November 1, 2024, Melbourne, Australia. ACM, New York, NY, USA, 13 pages. <https://doi.org/10.1145/3664647.3680647>

1 INTRODUCTION

Achieving high-level performance in deep representation learning typically requires large datasets, detailed labeling processes, and significant supervisory involvement. This requirement becomes even more daunting as the complexity of downstream tasks increases, challenging the scalability of supervised representation learning methods. In contrast, human learning is remarkably efficient, managing to acquire new skills from minimal examples with little supervision. Few-shot learning (FSL) [35, 42, 43, 48, 50, 51, 58, 62] aims to narrow this gap between human and machine learning capabilities. Although FSL has shown promising results in supervised settings, its dependence on extensive supervision remains a significant limitation. To address this, unsupervised FSL (U-FSL) [11, 34, 35] has been developed, mirroring the structure of supervised approaches. It involves pretraining on a wide dataset of base classes and then quickly adapting to novel, few-shot tasks [8]. The primary goal of U-FSL pretraining is to develop a feature extractor that understands the global structure of unlabeled data, and subsequently tailors the encoder for new tasks. The increasing interest in U-FSL reflects its practicality and alignment with self-supervised learning methods,

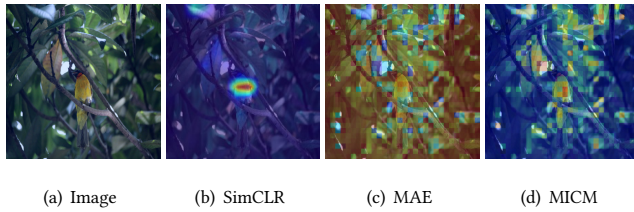


Figure 1: Illustrating the attention map with SimCLR [10] (CL), MAE [24] (MIM), MICM.

emphasizing its potential to significantly enhance machine learning processes.

Recent advancements in state-of-the-art (SOTA) methods have largely employed Contrastive Learning (CL) [11, 34, 35, 56, 57], particularly in transfer-learning scenarios. These methods have achieved impressive results across various benchmarks. As illustrated in Figure 2(a), the principle of contrastive representation learning [10] involves drawing ‘positive’ samples closer and pushing ‘negative’ ones away in the representation space. This technique focuses on specific objects within datasets, thus improving representational learning for image classification tasks, as depicted in Figure 1(b). Conversely, Masked Image Modeling (MIM) [13, 24] (Figure 2(b)) trains models to predict the original content of intentionally obscured image portions. This approach facilitates comprehensive learning of features across all image patches, including peripheral ones, as shown in Figure 1(c). In our research, we quantitatively assessed the impacts of MIM and CL on FSL tasks, revealing that *while CL prepares models to prioritize features typical in training datasets, potentially compromising reliability in novel categories, and MIM fosters a broad and generalized understanding of image features but struggles to develop discriminative features crucial for accurately categorizing new classes in few-shot scenarios.*

To explore the trade-offs between generalization and discriminability in unsupervised pretraining, we introduce Masked Image Contrastive Modeling (MICM), a novel method that ingeniously combines essential aspects of both CL and MIM to boost downstream inference performance. Illustrated in Figure 2(c), MICM utilizes an encoder-decoder architecture akin to MIM but integrates a decoder that simultaneously enhances features and reconstructs images. This method not only merges contrastive learning with effective pretext task designs but also adapts efficiently to downstream task data. We further introduce a U-FSL framework with two phases: *Unsupervised Pretraining* and *Few-Shot Learning*. During *Unsupervised Pretraining*, MICM blends CL and MIM objectives in a hybrid training strategy. In the *Few-Shot Learning* phase, MICM adapts to various few-shot strategies, both inductive and transductive. Extensive experimental analysis confirms the benefits of MICM, showing it significantly enhances both the generalization and discrimination capabilities of pre-trained models, achieving top-tier performance on multiple U-FSL datasets.

To summarize, the main contributions of our paper are as follows:

- We reveal the limitations of MIM and CL in terms of discriminative and generalization abilities, respectively, to their consequent underperformance in U-FSL contexts.

- We propose Masked Image Contrastive Modeling (MICM), a novel structure that blends the targeted object learning prowess of CL with the generalized visual feature learning capability of MIM.
- Extensive quantitative and qualitative results show that our method achieves SOTA performance on several In-Domain and Cross-Domain FSL datasets.

2 RELATED WORK

2.1 Few-Shot Learning

Few-shot learning (FSL) in visual classification contends with the challenge of recognizing objects from very limited samples. Primarily, this task is approached through two principal methodologies: transfer learning and meta-learning. Transfer learning, as discussed by Tian et al. [43], leverages knowledge from models pre-trained on large datasets to adapt to new, less-represented tasks. Meta-learning, alternatively, encompasses several strategies: model-based [6], metric-based [41], and optimization-based [1]. Model-based approaches focus on adapting the model parameters rapidly for new tasks. Metric-based methods compute distances between samples to facilitate class differentiation, while optimization-based strategies aim to maximize learning efficiency with scarce examples. Building upon inductive FSL, transductive FSL seeks to enhance real-world application by incorporating unlabeled data into the learning process for pre-classification tuning. Among the various techniques employed, graph-based methods such as protoLP [61] utilize graph structures to strengthen the information flow and relationships between support and query samples. Clustering-based approaches, exemplified by EASY [4], Transductive CNAPS [3], and BAVARDAGE [28], refine feature representations using advanced clustering techniques. Additionally, applications of the Optimal Transport Algorithm, like BECLR [35], are used to align feature distributions more effectively during testing phases. A novel approach, TRIDENT [40], integrates a unique variational inference network to enhance image representation in FSL scenarios.

2.2 Unsupervised Few-Shot Learning

U-FSL broadens the scope of unsupervised learning by requiring models to not only learn data representations without supervision but also to rapidly adapt to new few-shot tasks. This challenging dual requirement has led to the exploration of various innovative methods. Knowledge distillation and contrastive learning are notably effective in U-FSL, enhancing model adaptability through robust feature representations [29]. Furthermore, clustering-based approaches have demonstrated considerable success by optimizing data groupings to better model task-specific nuances [33]. Despite these advancements, many traditional unsupervised methods are geared towards batch data processing, which may not seamlessly translate to the dynamic requirements of few-shot scenarios. To mitigate this, some strategies integrate meta-learning principles to generate synthetic training scenarios that improve data efficiency and model responsiveness [2]. However, such approaches can sometimes lead to suboptimal data usage [20]. Recent innovations in U-FSL also include the use of graph-based structures to map relationships within data [9], the application of Structural Causal Models (SCM) in the context-aware multi-variational autoencoder

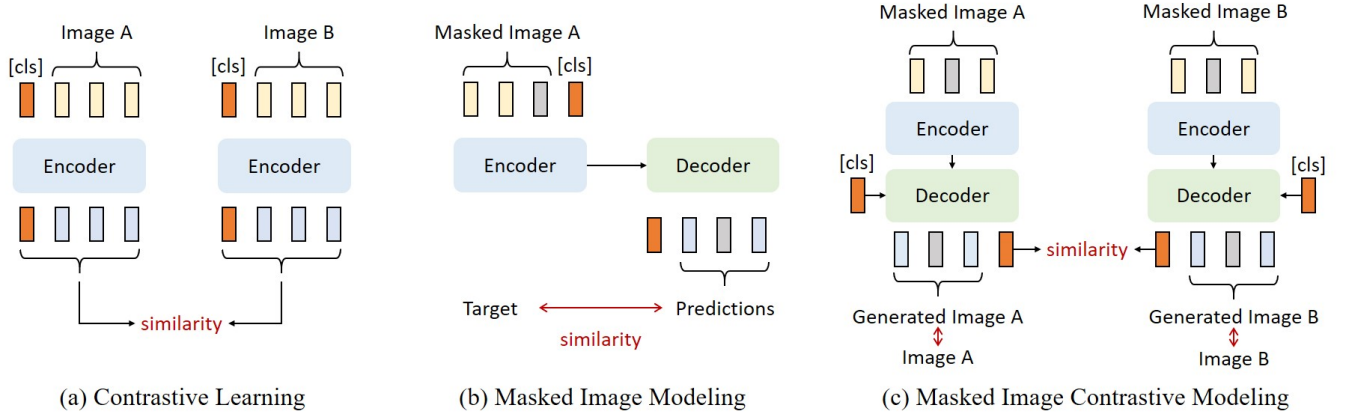


Figure 2: (a) *Contrastive Learning* is dedicated to learning discriminative data representations by contrasting and differentiating between similar (positive) and dissimilar (negative) pairs of data samples. This approach emphasizes the relative comparison to achieve distinctiveness in the learned features. (b) *Masked Image Modeling* involves training a model to accurately predict the original content of intentionally obscured (masked) portions of images. This technique focuses on learning comprehensive and robust feature representations by encouraging the model to infer missing information. (c) *Masked Image Contrastive Modeling* implements a decoder that simultaneously enhances features and reconstructs the original content of images. This method synergistically merges the principles of contrastive representation learning with effective pretext task design, thereby integrating the strengths of both approaches to achieve more nuanced and effective learning.

(CMVAE) [36], and the deployment of variational autoencoders (VAE) in frameworks like CMVAE and Meta-GMVAE [31]. Additionally, the exploration of rotation invariance in self-supervised learning enriches the robustness of models against geometric variations in few-shot learning tasks [51]. Another notable approach is MISO, which leverages multi-level visual abstraction features combined with power-normalized second-order base learner streams to enhance the discriminative capability of models in U-FSL [55].

3 QUALITATIVE STUDY ON UNSUPERVISED PRETRAINING METHODS FOR U-FSL

This section delves into Unsupervised Few-Shot Learning (U-FSL), elucidating the task and assessing the impact of different unsupervised pretraining methodologies on model performance.

3.1 Unsupervised Few-shot Learning

U-FSL operates under a widely recognized protocol delineated in recent work [11, 29, 34, 35]. Initially, models undergo an unsupervised pretraining phase using a vast unlabeled dataset $D_{\text{base}} = \{\mathbf{x}_i\}$, which encompasses a variety of *base* classes. Subsequently, the models are tested in a few-shot inference phase using a smaller, labeled test dataset $D_{\text{novel}} = \{(\mathbf{x}_i, \mathbf{y}_i)\}$ comprising *novel* classes, ensuring no overlap exists between the base and novel classes. Each few-shot task \mathcal{T}_i is structured around a support set $\mathcal{S} = \{(\mathbf{x}_i^{\mathcal{S}}, \mathbf{y}_i^{\mathcal{S}})\}_{i=1}^{NK}$, adhering to the (N -way, K -shot) scheme, where K labeled examples from N distinct classes are chosen. The query set $\mathcal{Q} = \{\mathbf{x}_j^{\mathcal{Q}}\}_{j=1}^{NQ}$, typically unlabeled, comprises NQ samples (where $Q > K$) and serves to evaluate the model’s adaptation to novel classes.

3.2 Unsupervised Pretraining Methods

The foundation of U-FSL is significantly influenced by the capabilities of unsupervised pretraining methods to discern intricate patterns within unlabeled datasets. This segment explores the effects of two principal unsupervised pretraining strategies: Contrastive Learning (CL) and Masked Image Modeling (MIM). Key exemplars for these methods—SimCLR [10] for CL and MAE [24] for MIM—were selected due to their prominence and efficacy. Both methodologies were implemented using the Vision Transformer Small (ViT-S) architecture on the MiniImageNet dataset. Our analytical focus is directed towards understanding how these pretraining approaches modify the model’s capability to transition effectively to novel tasks. We postulate that the intrinsic nature of the pretraining method—contrastive, which underscores learning distinctive features that delineate classes, versus masked, which centers on reconstructing absent segments of the input—will manifest differing strengths within the context of few-shot learning.

Analysis of Contrastive Learning. Recent research [13] has demonstrated that CL models tend to focus predominantly on the primary objects within images during pretraining. This concentration frequently targets small, distinct features that distinctly characterize the primary categories. Such specificity, while beneficial for initial categorization tasks, adversely affects the generalizability of the learned features to new, unseen contexts, as evidenced in Figure 1(b). We propose that this limitation arises from the inherent design of CL methodologies, which predispose the model to emphasize features that are salient in the training dataset but may be less relevant or even misleading in novel categories. To explore this proposition, we conducted empirical analyses comparing the feature representations of base category prototypes with those of novel category prototypes, both before and after applying SimCLR and its subsequent fine-tuning. The results, depicted in Figure 3,

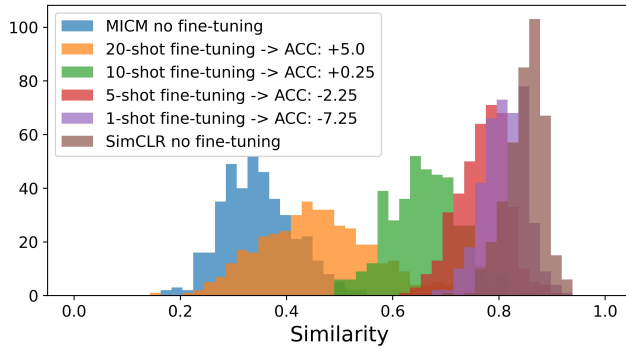


Figure 3: Histograms depicting the distribution of similarity between features extracted by the model for novel and base classes. Our model (blue) extracts distinctive features for novel classes, contrasting with the SimCLR model from contrastive learning methods, which continues to focus on discriminative features of base classes for novel classes, resulting in similar features (brown). Fine-tuning with an adequate number of labeled samples is essential to address these issues in SimCLR and enhance classification accuracy.

indicate that the features extracted for novel categories by SimCLR closely mirror those associated with the base categories. This similarity persists when models trained via CL are applied to novel categories, leading to a continued reliance on the same features identified during the training phase. Consequently, there is a notable deficiency in the model’s focus on principal objects in new categories, which hampers its adaptability. Building on established protocols [10, 16], we fine-tuned the SimCLR-trained models on downstream few-shot classification tasks. Our findings, illustrated in Figure 3, show that fine-tuning with a minimal set of labeled examples (e.g., in one-shot learning scenarios) fails to adequately rectify these issues of transferability. In some instances, this approach may even degrade the model’s performance on few-shot classification tasks. It becomes apparent that only with an ample number of labeled samples for fine-tuning do these challenges begin to mitigate, consequently improving accuracy in few-shot classification scenarios. This highlights the intrinsic difficulties of directly applying CL models to few-shot learning tasks, especially considering the heightened risk of overfitting when training data are scarce. Hence, we assert the following conclusion concerning the impact of contrastive learning:

Conclusion and Discussion. Contrastive learning fundamentally predisposes models to prioritize features that are prominent in the training dataset, potentially at the expense of relevance and utility in novel categories.

Analysis of Masked Image Modeling. Recent advancements in MIM underscore a shift towards a more comprehensive feature extraction methodology, distinct from techniques that prioritize prominent image features. As detailed in [13], MIM methods like the MAE engage systematically with every image patch to reconstruct absent segments, fostering a broad spatial activation across the entire image. This approach is vividly illustrated in Figure 1(c), where feature maps from MAE reveal a widespread distribution

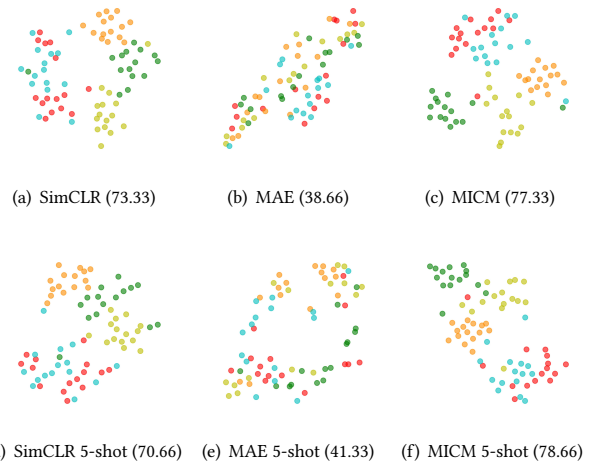


Figure 4: Visualization of t-SNE features for various unsupervised pre-trained models in novel categories. The first row: before fine-tuning. The second row: after fine-tuning with 5-shot. Contrary to SimCLR and MICM, the MAE method lacks discriminative features both prior to and following few-shot learning. The performance of each model in FSL is indicated in parentheses.

of activation, suggesting a more holistic grasp of image features. Despite these strengths, the extensive focus on patch reconstruction in MIM can obscure class-specific feature delineation. Since MIM models are optimized for predicting missing image parts rather than distinguishing class features, they frequently lack the sharp, discriminative capabilities essential for class-specific recognition tasks. This deficiency is apparent in Figure 4, where the first row demonstrates that features extracted by MAE are markedly less discriminative than those derived from our proposed method or the contrastive learning approach, SimCLR. The adaptability of MIM techniques to FSL scenarios is also challenged when these models are fine-tuned with limited labeled data. The second row of Figure 4 indicates that, even after fine-tuning with a modest sample size, such as in a 5-shot scenario, the discriminability of the features shows minimal enhancement. This observation implies that while MIM effectively encodes a rich array of generic visual features, it struggles to capture the subtleties required for distinguishing novel classes in few-shot configurations.

Conclusion and Discussion. While MIM techniques cultivate a broad and generalized understanding of image features, they encounter significant obstacles in acquiring discriminative features crucial for accurately categorizing novel classes in few-shot learning scenarios.

4 MASKED IMAGE CONTRASTIVE MODELING

The preceding comparative analysis in Section 3 elucidates that while CL prioritizes refining focus on distinct objects within datasets, enhancing representational efficacy for image classification, MIM extends its reach to a comprehensive understanding across all image patches, thus facilitating a broader scope of feature extraction. This

delineation underscores a pivotal trade-off in unsupervised pretraining between generalization and discriminability. To bridge this gap, we introduce a novel approach, Masked Image Contrastive Modeling (MICM), which amalgamates the strengths of both methodologies to foster robust representation learning coupled with an effective FSL task.

4.1 Model Structure

Figure 2 illustrates the encoder-decoder architecture of MICM, ingeniously designed to predict masked patches based on visible ones within the encoded space, while concurrently ensuring similar tokens for identical images are decoded effectively. The image undergoes segmentation into visible patches X_v and masked patches X_m . The encoder \mathcal{F} processes X_v to generate latent representations Z_v , while the decoder \mathcal{G} aims to reconstruct X_m using these encoded representations along with a predefined class token T_c .

Encoder. The encoder \mathcal{F} transforms visible patches X_v into latent representations Z_v . Utilizing the ViT as its backbone, the encoder begins by embedding the visible patches, projecting each patch linearly to create a set of embeddings. Positional embeddings P_v are added to maintain spatial context. These embeddings undergo processing through several transformer blocks, leveraging self-attention mechanisms to produce the latent representations Z_v , which encapsulate the critical features of the visible patches.

Decoder. The decoder serves dual functions in MICM. Its primary role is to transform the latent representations of visible patches Z_v and, crucially, those of masked patches Z_m back into the reconstructed patches Y_m . This transformation process entails a sequence of transformer blocks culminating in a linear layer that precisely regenerates the original masked patches. Secondly, the decoder also refines the input class token $Z_{[cls]}$ into an enhanced representation $\hat{Z}_{[cls]}$, pivotal for effective CL. Diverging from conventional approaches, MICM strategically delays the integration of the class token until the decoding phase, permitting the encoder to concentrate more thoroughly on capturing the nuances of visible patches. This structural delineation enhances the encoder’s focus on extracting a diverse array of visual features, while the decoder, through feature reconstruction, fine-tunes the class token, synergistically balancing the model’s objectives of maximizing discriminability and ensuring comprehensive feature extraction.

4.2 U-FSL with MICM

Unsupervised Pretraining. Given an input image x uniformly sampled from the training set D_{base} , we apply random data augmentations to create two distinct views x^1 and x^2 . These views are subsequently processed by the teacher and student networks, parameterized by θ^t and θ^s , respectively. Notably, the teacher network is updated via an Exponentially Moving Average (EMA) of the student network, facilitating knowledge transfer by minimizing the cross-entropy loss between the output categorical distributions of their augmented token representations, as expressed in the following equation:

$$\mathcal{L}_{[cls]} = \mathcal{H}(\hat{Z}_{[cls]}^t, \hat{Z}_{[cls]}^s), \quad (1)$$

where $\mathcal{H}(x, y) = -x \log y$, and $\hat{Z}_{[cls]}$ denotes the output class token. For MIM, we implement self-distillation as proposed in [59].

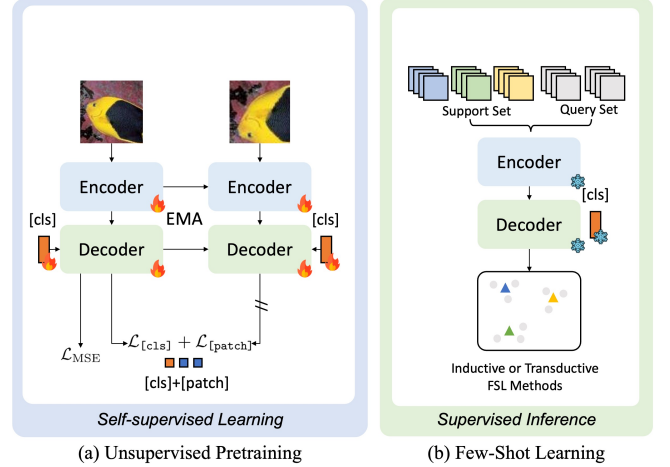


Figure 5: (a) The Unsupervised Pretraining phase involves self-supervised learning on a large, unlabeled base dataset, crucial for developing initial representations. (b) The Few-Shot Learning phase could adapt to a variety of few-shot learning approaches, including both inductive and transductive methodologies.

A random mask sequence $m \in \{0, 1\}^M$ is applied over an image with $N_{[patch]}$ tokens $x = \{x_i\}_{i=1}^M$. The masked patches, denoted by $m_i = 1$, are replaced by a learnable token embedding Z_m , resulting in a corrupted image \hat{x} . The student and teacher networks receive the corrupted and original uncorrupted images, respectively, to recover the masked tokens. This is quantified by minimizing the cross-entropy loss between their categorical distributions on masked patches:

$$\mathcal{L}_{[patch]} = \sum_{i=1}^M m_i \cdot \mathcal{H}(\hat{Z}_{[patch\ i]}^t, \hat{Z}_{[patch\ i]}^s). \quad (2)$$

Moreover, we aim for the decoder-generated tokens to predict the RGB information of the image, incorporating an image reconstruction loss using Mean Squared Error (MSE) for the reconstruction targets \bar{Y} :

$$\mathcal{L}_{MSE} = \sum (Y_m, \bar{Y}_m)^2. \quad (3)$$

Few-shot Learning. During the few-shot learning phase, the MICM approach is adeptly configured to adapt to diverse few-shot learning strategies, encompassing both inductive and transductive methods. The MICM methodology enhances feature learning by emphasizing generality across base classes and discriminative power. This dual capability significantly boosts the transferability of the learned features to few-shot tasks, thereby enabling superior adaptation to scenarios with limited labeled data. Further exploration of this adaptability is discussed in subsequent sections.

5 EXPERIMENTS

5.1 Datasets

Unsupervised few-shot recognition experiments are conducted on three benchmark datasets widely recognized in the field: MiniImageNet [44], TieredImageNet [37], and CIFAR-FS [5]. MiniImageNet,

Table 1: Accuracies (in % \pm standard deviation) on miniImageNet, comparing our model with various unsupervised pre-training methods (all models use VIT-S as backbone). CTB denotes the strategy of inserting a classification *cls token* before the processing by the encoder.

| Method | Setting | Inductive (ProtoNet) [41] | | Transductive (OpTA) [35] | |
|--------------------|---------------|----------------------------------|----------------------------------|----------------------------------|----------------------------------|
| | | 5-way 1-shot | 5-way 5-shot | 5-way 1-shot | 5-way 5-shot |
| SimCLR [10] | CL | 54.30 \pm 0.62 | 75.03 \pm 0.35 | 65.83 \pm 0.64 | 78.09 \pm 0.40 |
| MoCo V3 [25] | CL | 56.06 \pm 0.43 | 76.78 \pm 0.33 | 71.45 \pm 0.64 | 82.04 \pm 0.35 |
| MAE [24] | MIM | 29.11 \pm 0.44 | 37.01 \pm 0.31 | 25.36 \pm 0.48 | 35.21 \pm 0.42 |
| CAE [13] | MIM | 57.33 \pm 0.46 | 79.25 \pm 0.33 | 70.34 \pm 0.67 | 81.36 \pm 0.39 |
| iBOT [59] | MIM | 60.93 \pm 0.21 | 80.38 \pm 0.16 | 74.58 \pm 0.66 | 83.95 \pm 0.34 |
| MICM w/ CTB | MIM+CL | 62.85\pm0.17 | 82.37\pm0.11 | 77.89\pm0.62 | 86.36\pm0.33 |
| MICM | MIM+CL | 60.78\pm0.19 | 81.39\pm0.14 | 78.40\pm0.61 | 86.90\pm0.33 |

derived from the larger ILSVRC-12 dataset [38], consists of 100 categories, each represented by 600 images. It is divided into meta-training, meta-validation, and meta-testing segments, containing 64, 16, and 20 categories, respectively. TieredImageNet, also a subset of ILSVRC-12, includes 608 categories segmented into 351, 97, and 160 categories for training, validation, and testing. CIFAR-FS, a subset of CIFAR100 [30], follows a similar structure to MiniImageNet, with 60,000 images spread across 100 categories. These datasets provide a robust framework for evaluating few-shot learning algorithms. Additionally, cross-domain experiments use MiniImageNet as the pretraining (source) dataset and ISIC [17], EuroSAT [26], and CropDiseases [46] as inference (target) datasets, enhancing the generalizability assessment of the models.

5.2 Analysis of MICM

Discriminative and Generalization Capabilities. We investigate the critical balance between generalization and discriminability in unsupervised pretraining through our proposed MICM model. As depicted in Figure 6, MICM surpasses other unsupervised pretraining methods in capturing comprehensive object information from novel classes, exhibiting superior overall perception. This is further corroborated by the distance distribution between the prototypes of novel and base classes in Figure 3, where MICM’s prototypes distinctly differ more from the base class, affirming its enhanced generalization for novel classes. Additionally, Figure 4 demonstrates MICM’s superior discriminative capabilities compared to models like MAE, with a clearer distinction in feature distributions between MICM and SimCLR. Notably, MICM maintains leading performance in small-sample scenarios, both pre- and post-fine-tuning. The experimental validations highlight MICM’s adept integration of the strengths of CL and MIM, achieving remarkable discriminability and generalization.

Improving FSL. Our exploration focuses on the synergy between MIM and CL, designed to overcome the limitations inherent to each approach individually. The MICM model we introduce effectively integrates the strengths of these methodologies, emphasizing the extraction of relevant feature scales within images. This integration not only enhances category discrimination but also bolsters robustness in subsequent FSL tasks. The effectiveness of MICM is demonstrated through its superior performance in both inductive and transductive few-shot classification settings, detailed in Table 1.

Table 2: Accuracies (in % \pm std) on miniImageNet \rightarrow CUB., comparing our model with various unsupervised pretraining methods (all models use VIT-S as backbone). CTB denotes the strategy of inserting a classification *cls token* before the processing by the encoder.

| Method | Setting | Inductive (ProtoNet) [41] | | Transductive (OpTA) [35] | |
|--------------------|---------------|----------------------------------|----------------------------------|----------------------------------|----------------------------------|
| | | 5-way 1-shot | 5-way 5-shot | 5-way 1-shot | 5-way 5-shot |
| SimCLR [10] | CL | 39.80 \pm 0.32 | 55.72 \pm 0.37 | 38.99 \pm 0.40 | 53.09 \pm 0.42 |
| MoCo V3 [25] | CL | 42.12 \pm 0.33 | 59.33 \pm 0.37 | 41.83 \pm 0.41 | 57.36 \pm 0.42 |
| MAE [24] | MIM | 30.13 \pm 0.25 | 37.94 \pm 0.31 | 25.37 \pm 0.25 | 31.89 \pm 0.32 |
| CAE [13] | MIM | 38.10 \pm 0.43 | 51.56 \pm 0.53 | 38.31 \pm 0.56 | 49.01 \pm 0.58 |
| iBOT [59] | MIM | 42.71 \pm 0.33 | 59.33 \pm 0.38 | 43.30 \pm 0.43 | 58.56 \pm 0.43 |
| MICM w/ CTB | MIM+CL | 45.06\pm0.34 | 62.83\pm0.37 | 46.85\pm0.45 | 62.75\pm0.42 |
| MICM | MIM+CL | 44.95\pm0.34 | 63.05\pm0.37 | 47.42\pm0.46 | 63.86\pm0.42 |

Table 3: Accuracies (in % \pm standard deviation) on miniImageNet, comparing our model with various unsupervised pretraining methods, which are adapted to several FSL methods [12, 35, 41, 47, 52].

| Pretrained Model | FSL method | 5-way 1-shot | 5-way 5-shot |
|------------------|------------------|------------------------------------|------------------------------------|
| MAE [24] | ProtoNet [41] | 28.88 \pm 0.43 | 37.19 \pm 0.51 |
| SimCLR [10] | | 54.42 \pm 0.66 | 75.03 \pm 0.35 |
| iBOT [59] | | 61.26 \pm 0.66 | 80.64 \pm 0.45 |
| MICM | | 61.37 \pm 0.62 | 81.68 \pm 0.43 |
| MAE [24] | Fine-tuning [12] | 28.50 \pm 0.32 | 38.29 \pm 0.50 |
| SimCLR [10] | | 54.47 \pm 0.59 | 75.01 \pm 0.36 |
| iBOT [59] | | 61.11 \pm 0.59 | 80.91 \pm 0.39 |
| MICM | | 61.41 \pm 0.52 | 81.72 \pm 0.32 |
| MAE [24] | SimpleShot [47] | 30.30 \pm 0.47 | 38.65 \pm 0.50 |
| SimCLR [10] | | 57.13 \pm 0.64 | 74.88 \pm 0.46 |
| iBOT [59] | | 61.98 \pm 0.65 | 80.56 \pm 0.45 |
| MICM | | 62.53 \pm 0.63 | 81.79 \pm 0.43 |
| MAE [24] | DC [52] | 37.06 \pm 0.47 | 52.95 \pm 0.51 |
| SimCLR [10] | | 60.86 \pm 0.58 | 75.79 \pm 0.39 |
| iBOT [59] | | 65.84 \pm 0.67 | 83.77 \pm 0.43 |
| MICM | | 67.19 \pm 0.65 | 85.12 \pm 0.41 |
| MAE [24] | OpTA [35] | 25.36 \pm 0.48 | 35.21 \pm 0.42 |
| SimCLR [10] | | 65.83 \pm 0.64 | 78.09 \pm 0.40 |
| iBOT [59] | | 74.58 \pm 0.66 | 83.95 \pm 0.34 |
| MICM | | 78.40 \pm 0.61 | 86.90 \pm 0.33 |

Enhancing Cross-Domain FSL. In cross-domain scenarios, MICM also significantly excels, notably on the CUB dataset (Table 2). Unlike traditional CL models, which often overfit to base classes, MICM maintains generalization across varied domains without the need for fine-tuning, as illustrated in Figures 3 and 4. This capability underscores MICM’s effectiveness in capturing discernible features within an optimal range, thus boosting its adaptability and classification performance in few-shot learning across different domains. **Broad Adaptation to FSL Methods.** As a versatile pre-training model, MICM adapts seamlessly across a spectrum of FSL strategies. Comprehensive evaluations show that MICM invariably boosts performance, with notable improvements such as a nearly 4% enhancement over the iBOT model when utilizing the transductive

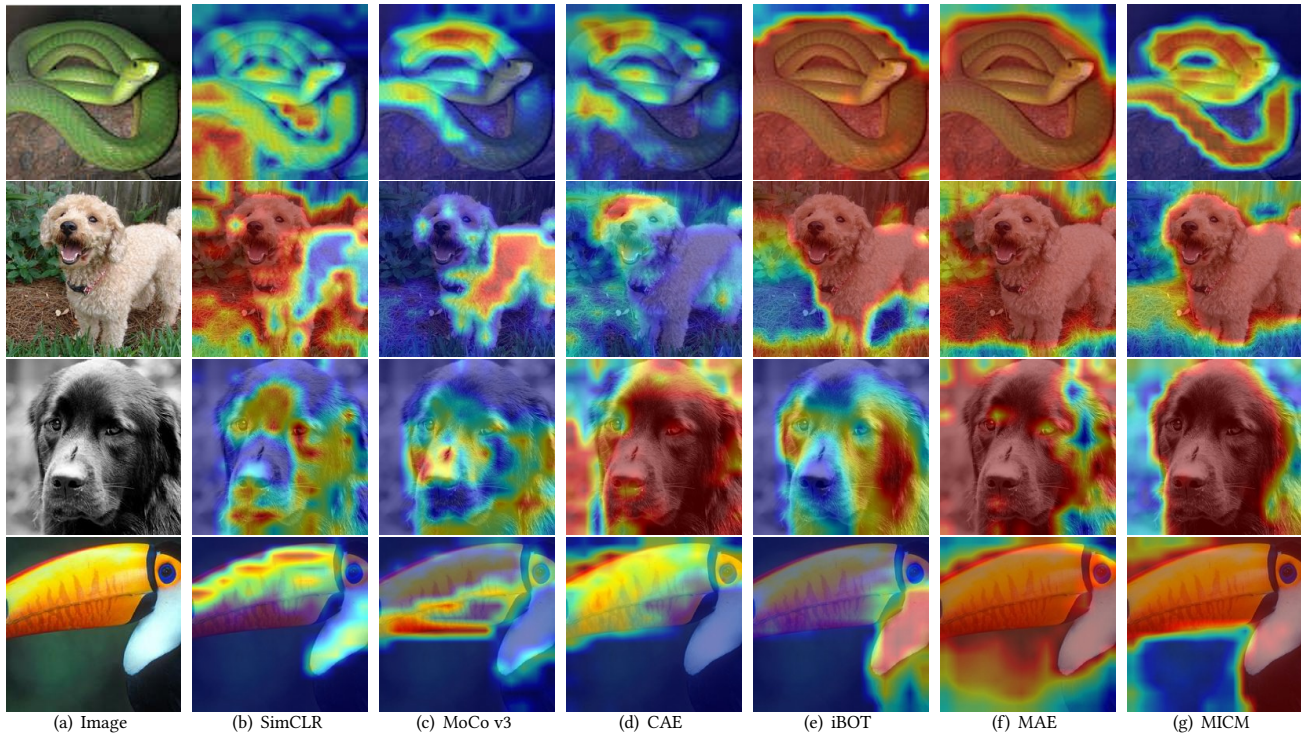


Figure 6: Attention map visualization for different unsupervised pre-trained models. This figure presents a series of columns, each corresponding to the attention map output from a distinct model. From left to right, the columns are as follows: (a) the original image; (b) SimCLR [10]; (c) Moco v3 [16]; (d) CAE [13]; (e) iBOT [60]; (f) MAE [24]; and (g) MICM (ours).

method OpTA. These results affirm the robust generalization ability of MICM across a range of FSL approaches.

cls token Variation. In exploring variations, we introduced a *cls token* as an input to the Encoder, with performance outcomes detailed in Tables 1 and 2. Although this variant achieves commendable results in the inductive setting, it does not outperform the configuration where the *cls token* is input into the Decoder, especially in transductive scenarios. This suggests that introducing the *cls token* early in the encoder may impede the encoder’s ability to learn comprehensive visual features effectively. Conversely, positioning the *cls token* in the decoder helps alleviate potential negative impacts by CL on learning holistic visual features.

5.3 Comparison with SOTA Method

To assess the efficacy of MICM in FSL scenarios, particularly under the U-FSL framework, we developed and evaluated a novel methodology that combines unsupervised pre-training with pseudo-label training techniques. We integrated pseudo-label learning [35] with the transductive OpTA FSL method [35], forming a hybrid approach designed to leverage the combined strengths of these methods to boost performance in scenarios with scarce labeled data. Our method’s performance was benchmarked against SOTA models across various datasets, with detailed methodological descriptions provided in the Appendix.

In-Domain Setting. Our model was evaluated against a broad range of baselines including established SSL baselines [7, 10, 15, 21, 22, 54], prominent U-FSL methods [9, 11, 27, 29, 34, 39], leading supervised FSL approaches [3, 32], and a recent transductive U-FSL model [35]. Our model demonstrates superior performance, outperforming both inductive and transductive U-FSL methods as evidenced in Tables 4 and 5, showing a notable accuracy improvement on the CIFAR-FS dataset.

Our implementation utilizes the ViT architecture, which contrasts with the commonly used ResNet in U-FSL studies. To facilitate comprehensive evaluation, we compared results from models using both ResNet18 and ResNet50 architectures, and additionally, we benchmarked against a ViT-S model trained using the MIM method for transductive classification (MIM+OpTA), providing a baseline for ViT-based transductive U-FSL models.

Regarding CIFAR-FS performance comparisons (Table 5), sourced from [35], we note that the BECLR model reported results using ResNet18. Hence, our model’s reported performance is achieved with a scaled-down version of ViT-S, comprising 6 layers (4 encoder layers and 2 decoder layers) as opposed to the full 12 layers in standard ViT-S.

Cross-Domain Setting. Following established methodologies [23, 35], we pretrained on the minilmageNet dataset and evaluated our approach in cross-domain few-shot learning settings. The results, detailed in Table 6, demonstrate that MICM sets new SOTA

Table 4: Accuracies (in % \pm standard deviation) on miniImageNet and tieredImageNet, comparing our model with various baselines categorized into Inductive (Ind.) and Transductive (Transd.) approaches. Performance is delineated by backbone architectures, namely Residual Networks (RN) and Vision Transformers (ViT), with the number of parameters (Param) for each model included for an extensive comparison.

| Method | Backbone | Param | Setting | miniImageNet | | tieredImageNet | |
|-------------------------------|--------------------------------------|------------|----------------|------------------------------------|------------------------------------|------------------------------------|------------------------------------|
| | | | | 5-way 1-shot | 5-way 5-shot | 5-way 1-shot | 5-way 5-shot |
| SwAV [7] | RN18 ($\times 1$) | 11.2M | Ind. | 59.84 \pm 0.52 | 78.23 \pm 0.26 | 65.26 \pm 0.53 | 81.73 \pm 0.24 |
| NNCLR [21] | RN18 ($\times 2$) | 22.4M | Ind. | 63.33 \pm 0.53 | 80.75 \pm 0.25 | 65.46 \pm 0.55 | 81.40 \pm 0.27 |
| CPNWCP [45] | RN18 ($\times 1$) | 11.2M | Ind. | 53.14 \pm 0.62 | 67.36 \pm 0.5 | 45.46 \pm 0.19 | 62.96 \pm 0.19 |
| HMS [53] | RN18 ($\times 1$) | 11.2M | Ind. | 58.20 \pm 0.23 | 75.77 \pm 0.16 | 58.42 \pm 0.25 | 75.85 \pm 0.18 |
| SAMPTransfer [39] | RN18 ($\times 1$) | 11.2M | Ind. | 45.75 \pm 0.77 | 68.33 \pm 0.66 | 42.32 \pm 0.75 | 53.45 \pm 0.76 |
| PsCo [29] | RN18 ($\times 1$) | 11.2M | Ind. | 47.24 \pm 0.76 | 65.48 \pm 0.68 | 54.33 \pm 0.54 | 69.73 \pm 0.49 |
| PDA-Net [11] | RN50 ($\times 1$) | 23.5M | Ind. | 63.84 \pm 0.91 | 83.11 \pm 0.56 | 69.01 \pm 0.93 | 84.20 \pm 0.69 |
| UniSiam + dist [34] | RN50 ($\times 1$) | 23.5M | Ind. | 65.33 \pm 0.36 | 83.22 \pm 0.24 | 69.60 \pm 0.38 | 86.51 \pm 0.26 |
| Meta-DM + UniSiam + dist [27] | RN50 ($\times 1$) | 23.5M | Ind. | 66.68 \pm 0.36 | 85.29 \pm 0.23 | 69.61 \pm 0.38 | 86.53 \pm 0.26 |
| CPNWCP + OpTA [45] | RN18 ($\times 1$) | 11.2M | Transd. | 60.45 \pm 0.81 | 75.84 \pm 0.56 | 55.05 \pm 0.31 | 72.91 \pm 0.26 |
| HMS + OpTA [53] | RN18 ($\times 1$) | 11.2M | Transd. | 69.85 \pm 0.42 | 80.77 \pm 0.35 | 71.75 \pm 0.43 | 81.32 \pm 0.34 |
| PsCo + OpTA [29] | RN18 ($\times 1$) | 11.2M | Transd. | 52.89 \pm 0.71 | 67.42 \pm 0.54 | 57.46 \pm 0.59 | 70.70 \pm 0.45 |
| UniSiam + OpTA [34] | RN18 ($\times 1$) | 11.2M | Transd. | 72.54 \pm 0.61 | 82.46 \pm 0.32 | 73.37 \pm 0.64 | 73.37 \pm 0.64 |
| BECLR [35] | RN18 ($\times 2$) | 22.4M | Transd. | 75.74 \pm 0.62 | 84.93 \pm 0.33 | 76.44 \pm 0.66 | 84.85 \pm 0.37 |
| BECLR [35] | RN50 ($\times 2$) | 47M | Transd. | 80.57 \pm 0.57 | 87.82 \pm 0.29 | 81.69 \pm 0.61 | 87.82 \pm 0.32 |
| MICM | VIT-S ($\times 2$) | 42M | Transd. | 81.05 \pm 0.58 | 87.95 \pm 0.34 | 83.30 \pm 0.61 | 89.61 \pm 0.35 |

Table 5: Accuracies (in % \pm std) for CIFAR-FS dataset.

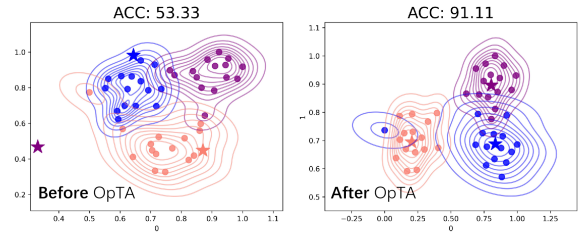
| Method | 5-way 1-shot | 5-way 5-shot |
|--------------|----------------------------------|----------------------------------|
| SimCLR [10] | 54.56 \pm 0.19 | 71.19 \pm 0.18 |
| MoCo v2 [14] | 52.73 \pm 0.20 | 67.81 \pm 0.19 |
| LF2CS [33] | 55.04 \pm 0.72 | 70.62 \pm 0.57 |
| HMS [53] | 54.65 \pm 0.20 | 73.70 \pm 0.18 |
| BECLR [35] | 70.39 \pm 0.62 | 81.56 \pm 0.39 |
| MICM | 79.20\pm0.61 | 86.35\pm0.39 |

Table 6: 5-way 5-shots accuracies (in % \pm std) on miniImageNet \rightarrow Cross-Domain Few-Shot Learning.

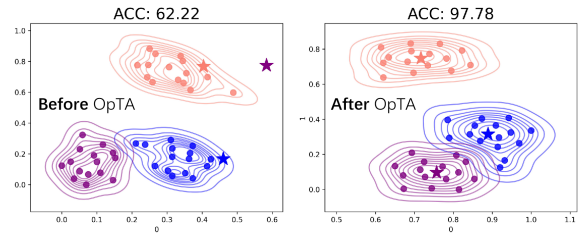
| Method | ChestX | ISIC | EuroSAT | CropDiseases | Mean |
|---------------------|------------------|------------------|------------------|------------------|-------|
| SwAV [7] | 25.70 \pm 0.28 | 40.69 \pm 0.34 | 84.82 \pm 0.24 | 88.64 \pm 0.26 | 60.12 |
| NNCLR [21] | 25.74 \pm 0.41 | 38.85 \pm 0.56 | 83.45 \pm 0.53 | 90.76 \pm 0.57 | 59.70 |
| SAMPTransfer [39] | 26.27 \pm 0.44 | 47.60 \pm 0.59 | 85.55 \pm 0.60 | 91.74 \pm 0.55 | 62.79 |
| PsCo [29] | 24.78 \pm 0.23 | 44.00 \pm 0.30 | 81.08 \pm 0.35 | 88.24 \pm 0.31 | 59.52 |
| UniSiam + dist [34] | 28.18 \pm 0.45 | 45.65 \pm 0.58 | 86.53 \pm 0.47 | 92.05 \pm 0.50 | 63.10 |
| ConFeSS [19] | 27.09 | 48.85 | 84.65 | 88.88 | 62.36 |
| BECLR [35] | 28.46 \pm 0.23 | 44.48 \pm 0.31 | 88.55 \pm 0.23 | 93.65 \pm 0.25 | 63.78 |
| MICM | 27.11 \pm 0.36 | 46.85 \pm 0.52 | 90.08 \pm 0.36 | 94.61 \pm 0.27 | 64.66 |

benchmarks on the EuroSAT and Crop Diseases datasets, while maintaining competitive performance on the ISIC dataset. MICM’s adaptive training mechanism enables superior performance over BECLR in cross-domain settings, highlighting its robustness and adaptability across diverse datasets.

Feature Distribution Analysis. To deepen our understanding of the MICM mechanism, we employed iBOT [59] as a baseline for



(a) iBOT [59]



(b) MICM

Figure 7: Feature distribution maps comparing various methods before and after applying OpTA.

comparative analysis. A critical observation, illustrated in Figure 7, is that MICM significantly enhances the compactness and cohesion of feature distributions within the same category. Compared to the baseline, where feature clusters are dispersed and misaligned (as shown in Figure 7(a)), our model demonstrates a notably tighter

clustering. This improvement is especially evident in the alignment of support samples with the corresponding query samples within each category. The application of the OpTA method notably rectifies sample bias, further refining feature distribution, and alignment. This adjustment, combined with the advanced feature representation capabilities of our MICM model, yields a substantial enhancement in performance relative to the baseline. The precise clustering of category-specific features and the effective mitigation of sample bias by OpTA underline the robustness and effectiveness of our model in generating highly discriminative feature representations, which is pivotal for few-shot learning applications.

6 CONCLUSION

In this paper, we have delineated the limitations of Masked Image Modeling (MIM) and Contrastive Learning (CL) in terms of their discriminative and generalization capabilities, which have contributed to their underperformance in Unsupervised Few-Shot Learning (U-FSL) contexts. To tackle these challenges, we introduced Masked Image Contrastive Modeling (MICM), a novel approach that effectively integrates the strengths of MIM and CL. Our results demonstrate that MICM adeptly balances discriminative power with generalizability, particularly in few-shot learning scenarios characterized by limited sample sizes. MICM's flexibility in adapting to various few-shot learning strategies highlights its potential as a versatile and powerful tool for unsupervised pretraining within the U-FSL framework. Extensive quantitative and qualitative evaluations show MICM's clear superiority over existing methods, confirming its ability to enhance feature discrimination, robustness, and adaptability across diverse few-shot learning tasks.

ACKNOWLEDGMENTS

This work is supported by the National Natural Science Foundation of China under grants 62206102, 62376103, 62302184, U1936108, 62025101, and 62088102; the Science and Technology Support Program of Hubei Province under grant 2022BAA046; the Postdoctoral Fellowship Program of CPSF under grants GZB20230024 and GZC20240035; and the China Postdoctoral Science Foundation under grant 2024M750100.

REFERENCES

- [1] Antreas Antoniou, Harrison Edwards, and Amos Storkey. 2018. How to train your MAML. *arXiv preprint arXiv:1810.09502* (2018).
- [2] Antreas Antoniou and Amos Storkey. 2019. Assume, augment and learn: Unsupervised few-shot meta-learning via random labels and data augmentation. *arXiv preprint arXiv:1902.09884* (2019).
- [3] Peyman Bateni, Jarred Barber, Jan-Willem Van de Meent, and Frank Wood. 2022. Enhancing few-shot image classification with unlabelled examples. In *Proceedings of the IEEE/CVF Winter Conference on Applications of Computer Vision*. 2796–2805.
- [4] Yassir Bendou, Yuqing Hu, Raphael Lafargue, Giulia Lioi, Bastien Pasdeloup, Stéphane Pateux, and Vincent Gripon. 2022. Easy—ensemble augmented-shot-y-shaped learning: State-of-the-art few-shot classification with simple components. *Journal of Imaging* 8, 7 (2022), 179.
- [5] Luca Bertinetto, Joao F Henriques, Philip HS Torr, and Andrea Vedaldi. 2018. Meta-learning with differentiable closed-form solvers. *arXiv preprint arXiv:1805.08136* (2018).
- [6] Qi Cai, Yingwei Pan, Ting Yao, Chenggang Yan, and Tao Mei. 2018. Memory matching networks for one-shot image recognition. In *Proceedings of the IEEE conference on computer vision and pattern recognition*. 4080–4088.
- [7] Mathilde Caron, Ishan Misra, Julien Mairal, Priya Goyal, Piotr Bojanowski, and Armand Joulin. 2020. Unsupervised learning of visual features by contrasting cluster assignments. *Advances in neural information processing systems* 33 (2020), 9912–9924.
- [8] Guangyao Chen, Peixi Peng, Yangru Huang, Mengyue Geng, and Yonghong Tian. 2024. Adaptive Discovering and Merging for Incremental Novel Class Discovery. In *Proceedings of the AAAI Conference on Artificial Intelligence*, Vol. 38. 11276–11284.
- [9] Kuilin Chen and Chi-Guhn Lee. 2022. Unsupervised Few-shot Learning via Deep Laplacian Eigenmaps. *arXiv preprint arXiv:2210.03595* (2022).
- [10] Ting Chen, Simon Kornblith, Mohammad Norouzi, and Geoffrey Hinton. 2020. A simple framework for contrastive learning of visual representations. In *International conference on machine learning*. PMLR, 1597–1607.
- [11] Wentao Chen, Chenyang Si, Wei Wang, Liang Wang, Zilei Wang, and Tieniu Tan. 2021. Few-shot learning with part discovery and augmentation from unlabeled images. *arXiv preprint arXiv:2105.11874* (2021).
- [12] Wei-Yu Chen, Yen-Cheng Liu, Zolt Kira, Yu-Chiang Frank Wang, and Jia-Bin Huang. 2019. A closer look at few-shot classification. *arXiv preprint arXiv:1904.04232* (2019).
- [13] Xiaokang Chen, Mingyu Ding, Xiaodi Wang, Ying Xin, Shentong Mo, Yunhao Wang, Shumin Han, Ping Luo, Gang Zeng, and Jingdong Wang. 2023. Context autoencoder for self-supervised representation learning. *International Journal of Computer Vision* (2023), 1–16.
- [14] Xinlei Chen, Haoqi Fan, Ross Girshick, and Kaiming He. 2020. Improved baselines with momentum contrastive learning. *arXiv preprint arXiv:2003.04297* (2020).
- [15] Xinlei Chen and Kaiming He. 2021. Exploring simple siamese representation learning. In *Proceedings of the IEEE/CVF conference on computer vision and pattern recognition*. 15750–15758.
- [16] X Chen, S Xie, and K He. [n. d.]. An empirical study of training self-supervised vision transformers. In 2021 IEEE. In *CVF International Conference on Computer Vision (ICCV)*, 9620–9629.
- [17] Noel Codella, Veronica Rotemberg, Philipp Tschandl, M Emre Celebi, Stephen Dusza, David Gutman, Brian Helba, Aadi Kalloo, Konstantinos Liopyris, Michael Marchetti, et al. 2019. Skin lesion analysis toward melanoma detection 2018: A challenge hosted by the international skin imaging collaboration (isic). *arXiv preprint arXiv:1902.03368* (2019).
- [18] Marco Cuturi. 2013. Sinkhorn distances: Lightspeed computation of optimal transport. *Advances in neural information processing systems* 26 (2013).
- [19] Debasmit Das, Sungrack Yun, and Fatih Porikli. 2021. ConfeSS: A framework for single source cross-domain few-shot learning. In *International Conference on Learning Representations*.
- [20] Guneet S Dhillon, Pratik Chaudhari, Avinash Ravichandran, and Stefano Soatto. 2019. A baseline for few-shot image classification. *arXiv preprint arXiv:1909.02729* (2019).
- [21] Debidatta Dwivedi, Yusuf Aytar, Jonathan Tompson, Pierre Sermanet, and Andrew Zisserman. 2021. With a little help from my friends: Nearest-neighbor contrastive learning of visual representations. In *Proceedings of the IEEE/CVF International Conference on Computer Vision*. 9588–9597.
- [22] Jean-Bastien Grill, Florian Strub, Florent Altché, Corentin Tallec, Pierre Richemond, Elena Buchatskaya, Carl Doersch, Bernardo Avila Pires, Zhaohan Guo, Mohammad Gheshlaghi Azar, et al. 2020. Bootstrap your own latent—a new approach to self-supervised learning. *Advances in neural information processing systems* 33 (2020), 21271–21284.
- [23] Yunhui Guo, Noel C Codella, Leonid Karlinsky, James V Codella, John R Smith, Kate Saenko, Tajana Rosing, and Rogerio Feris. 2020. A broader study of cross-domain few-shot learning. In *Computer Vision—ECCV 2020: 16th European Conference, Glasgow, UK, August 23–28, 2020, Proceedings, Part XXVII* 16. Springer, 124–141.

- [24] Kaiming He, Xinlei Chen, Saining Xie, Yanghao Li, Piotr Dollár, and Ross Girshick. 2022. Masked autoencoders are scalable vision learners. In *Proceedings of the IEEE/CVF conference on computer vision and pattern recognition*. 16000–16009.
- [25] Kaiming He, Haoqi Fan, Yuxin Wu, Saining Xie, and Ross Girshick. 2020. Momentum contrast for unsupervised visual representation learning. In *Proceedings of the IEEE/CVF conference on computer vision and pattern recognition*. 9729–9738.
- [26] Patrick Helber, Benjamin Bischke, Andreas Dengel, and Damian Borth. 2019. Eurosat: A novel dataset and deep learning benchmark for land use and land cover classification. *IEEE Journal of Selected Topics in Applied Earth Observations and Remote Sensing* 12, 7 (2019), 2217–2226.
- [27] Wentao Hu, Xiurong Jiang, Jiarun Liu, Yuqi Yang, and Hui Tian. 2023. Meta-DM: Applications of Diffusion Models on Few-Shot Learning. *arXiv preprint arXiv:2305.08092* (2023).
- [28] Yuqing Hu, Stéphane Pateux, and Vincent Gripon. 2023. Adaptive Dimension Reduction and Variational Inference for Transductive Few-Shot Classification. In *International Conference on Artificial Intelligence and Statistics*. PMLR, 5899–5917.
- [29] Huiwon Jang, Hankook Lee, and Jinwoo Shin. 2023. Unsupervised Meta-learning via Few-shot Pseudo-supervised Contrastive Learning. *arXiv preprint arXiv:2303.00996* (2023).
- [30] Alex Krizhevsky, Vinod Nair, and Geoffrey Hinton. 2010. Cifar-10 (canadian institute for advanced research). URL <http://www.cs.toronto.edu/kriz/cifar.html> 5, 4 (2010), 1.
- [31] Dong Bok Lee. 2021. Meta-GMVAE: Mixture of Gaussian VAEs for unsupervised meta-learning. (2021).
- [32] Kwonjoon Lee, Subhansu Maji, Avinash Ravichandran, and Stefano Soatto. 2019. Meta-learning with differentiable convex optimization. In *Proceedings of the IEEE/CVF conference on computer vision and pattern recognition*. 10657–10665.
- [33] Shuo Li, Fang Liu, Zehua Hao, Kaibo Zhao, and Licheng Jiao. 2022. Unsupervised few-shot image classification by learning features into clustering space. In *European Conference on Computer Vision*. Springer, 420–436.
- [34] Yuning Lu, Liangjian Wen, Jianzhuang Liu, Yajing Liu, and Xinmei Tian. 2022. Self-supervision can be a good few-shot learner. In *European Conference on Computer Vision*. Springer, 740–758.
- [35] Stelios Poulakakis Daktylidis. 2023. BECLR: Batch Enhanced Contrastive Unsupervised Few-Shot Learning. (2023).
- [36] Guodong Qi and Huimin Yu. 2023. CMVAE: Causal Meta VAE for Unsupervised Meta-Learning. *arXiv preprint arXiv:2302.09731* (2023).
- [37] Mengye Ren, Eleni Triantafyllou, Sachin Ravi, Jake Snell, Kevin Swersky, Joshua B Tenenbaum, Hugo Larochelle, and Richard S Zemel. 2018. Meta-learning for semi-supervised few-shot classification. *arXiv preprint arXiv:1803.00676* (2018).
- [38] Olga Russakovsky, Jia Deng, Hao Su, Jonathan Krause, Sanjeev Satheesh, Sean Ma, Zhiheng Huang, Andrej Karpathy, Aditya Khosla, Michael Bernstein, et al. 2015. Imagenet large scale visual recognition challenge. *International journal of computer vision* 115 (2015), 211–252.
- [39] Ojas Kishorkumar Shirekar, Anuj Singh, and Hadi Jamali-Rad. 2023. Self-Attention Message Passing for Contrastive Few-Shot Learning. In *Proceedings of the IEEE/CVF Winter Conference on Applications of Computer Vision*. 5426–5436.
- [40] Anuj Singh and Hadi Jamali-Rad. 2022. Transductive decoupled variational inference for few-shot classification. *arXiv preprint arXiv:2208.10559* (2022).
- [41] Jake Snell, Kevin Swersky, and Richard Zemel. 2017. Prototypical networks for few-shot learning. *Advances in neural information processing systems* 30 (2017).
- [42] Zeyin Song, Yifan Zhao, Yujun Shi, Peixi Peng, Li Yuan, and Yonghong Tian. 2023. Learning with fantasy: Semantic-aware virtual contrastive constraint for few-shot class-incremental learning. In *Proceedings of the IEEE/CVF conference on computer vision and pattern recognition*. 24183–24192.
- [43] Yonglong Tian, Yue Wang, Dilip Krishnan, Joshua B Tenenbaum, and Phillip Isola. 2020. Rethinking few-shot image classification: a good embedding is all you need?. In *Computer Vision—ECCV 2020: 16th European Conference, Glasgow, UK, August 23–28, 2020, Proceedings, Part XIV 16*. Springer, 266–282.
- [44] Oriol Vinyals, Charles Blundell, Timothy Lillicrap, Daan Wierstra, et al. 2016. Matching networks for one shot learning. *Advances in neural information processing systems* 29 (2016).
- [45] Haoqing Wang and Zhi-Hong Deng. 2022. Contrastive prototypical network with Wasserstein confidence penalty. In *European Conference on Computer Vision*. Springer, 665–682.
- [46] Xiaosong Wang, Yifan Peng, Le Lu, Zhiyong Lu, Mohammadhadi Bagheri, and Ronald M Summers. 2017. Chestx-ray8: Hospital-scale chest x-ray database and benchmarks on weakly-supervised classification and localization of common thorax diseases. In *Proceedings of the IEEE conference on computer vision and pattern recognition*. 2097–2106.
- [47] Yan Wang, Wei-Lun Chao, Kilian Q Weinberger, and Laurens Van Der Maaten. 2019. SimpleShot: Revisiting nearest-neighbor classification for few-shot learning. *arXiv preprint arXiv:1911.04623* (2019).
- [48] Zeyuan Wang, Yifan Zhao, Jia Li, and Yonghong Tian. 2020. Cooperative bi-path metric for few-shot learning. In *Proceedings of the 28th ACM international conference on multimedia*. 1524–1532.
- [49] Peter Welinder, Steve Branson, Takeshi Mita, Catherine Wah, Florian Schroff, Serge Belongie, and Pietro Perona. 2010. Caltech-UCSD birds 200. (2010).
- [50] Heng Wu, Yifan Zhao, and Jia Li. 2021. Selective, structural, subtle: Trilinear spatial-awareness for few-shot fine-grained visual recognition. In *2021 IEEE International Conference on Multimedia and Expo (ICME)*. IEEE, 1–6.
- [51] Heng Wu, Yifan Zhao, and Jia Li. 2023. Invariant and consistent: Unsupervised representation learning for few-shot visual recognition. *Neurocomputing* 520 (2023), 1–14.
- [52] Shuo Yang, Lu Liu, and Min Xu. 2021. Free lunch for few-shot learning: Distribution calibration. *arXiv preprint arXiv:2101.06395* (2021).
- [53] Han-Jia Ye, Lu Han, and De-Chuan Zhan. 2022. Revisiting unsupervised meta-learning via the characteristics of few-shot tasks. *IEEE Transactions on Pattern Analysis and Machine Intelligence* 45, 3 (2022), 3721–3737.
- [54] Jure Zbontar, Li Jing, Ishan Misra, Yann LeCun, and Stéphane Deny. 2021. Barlow twins: Self-supervised learning via redundancy reduction. In *International Conference on Machine Learning*. PMLR, 12310–12320.
- [55] Hongguang Zhang, Hongdong Li, and Piotr Koniusz. 2022. Multi-level second-order few-shot learning. *IEEE Transactions on Multimedia* (2022).
- [56] Ji Zhang, Lianli Gao, Xu Luo, Hengtao Shen, and Jingkuan Song. 2023. Deta: Denoised task adaptation for few-shot learning. In *Proceedings of the IEEE/CVF International Conference on Computer Vision*. 11541–11551.
- [57] Ji Zhang, Jingkuan Song, Lianli Gao, and Hengtao Shen. 2022. Free-lunch for cross-domain few-shot learning: Style-aware episodic training with robust contrastive learning. In *Proceedings of the 30th ACM International Conference on Multimedia*. 2586–2594.
- [58] Yifan Zhao, Tong Zhang, Jia Li, and Yonghong Tian. 2023. Dual adaptive representation alignment for cross-domain few-shot learning. *IEEE Transactions on Pattern Analysis and Machine Intelligence* 45, 10 (2023), 11720–11732.
- [59] Jinghao Zhou, Chen Wei, Huiyu Wang, Wei Shen, Cihang Xie, Alan Yuille, and Tao Kong. 2021. ibot: Image bert pre-training with online tokenizer. *arXiv preprint arXiv:2111.07832* (2021).
- [60] Jinghao Zhou, Chen Wei, Huiyu Wang, Wei Shen, Cihang Xie, Alan Yuille, and Tao Kong. 2021. Image BERT Pre-training with Online Tokenizer. In *International Conference on Learning Representations*.
- [61] Hao Zhu and Piotr Koniusz. 2023. Transductive Few-shot Learning with Prototype-based Label Propagation by Iterative Graph Refinement. In *Proceedings of the IEEE/CVF Conference on Computer Vision and Pattern Recognition*. 23996–24006.
- [62] Yixiong Zou, Shanghang Zhang, Guangyao Chen, Yonghong Tian, Kurt Keutzer, and José MF Moura. 2021. Annotation-Efficient Untrimmed Video Action Recognition. In *Proceedings of the 29th ACM International Conference on Multimedia*. 487–495.

In this Appendix, we present additional experimental results. Subsequently, we introduce an enhanced model of MICM, labeled as MICM+. Finally, we discuss the computational and storage costs associated with MICM.

1 Implementation Details

Self-Supervised Learning: The Vision Transformer (ViT) backbone and its associated projection head are pre-trained following the iBOT [59] framework, retaining most original hyper-parameters. The training employs a batch size of 640 and a learning rate of 0.0005 on a cosine decay schedule. The MiniImageNet and TieredImageNet datasets are pre-trained for 1200 epochs, while CIFAR-FS is pre-trained for 950 epochs. Additional training details are provided in the appendix.

Few-shot Evaluation: The pre-trained ViT backbone functions as the feature extractor. We utilize various few-shot learning (FSL) methods, including the prototypical networks approach [41], for evaluation. In each N-way K-shot task, class prototypes are calculated as the mean of the features from K support samples per class. Query images are then classified based on the highest cosine similarity to these prototypes. The feature set for evaluation combines the [cls] token with the weighted average [patch] token, using self-attention values from the last transformer layer. Test accuracies are reported over 2000 episodes, with each episode featuring 15 query shots per class, consistent with standard practices in the literature [11, 34, 35], and presented with 95% confidence intervals for all datasets.

A SUPPLEMENT TO FIGURE 3

Using the same configuration as in Figure 3, we have generated a comparable Figure 8 for the MAE model. We observe high similarity (above 0.9) between the features generated by the MAE for novel class samples and the prototypes of the base class. This high similarity remains even with limited samples available for fine-tuning, as illustrated in Figure 8 (right). The features of the MAE for base classes are indistinguishable, causing all prototypes to converge in the center of the feature space. Consequently, both novel and base class samples are extremely close to these central prototypes, resulting in indistinguishable classifications.

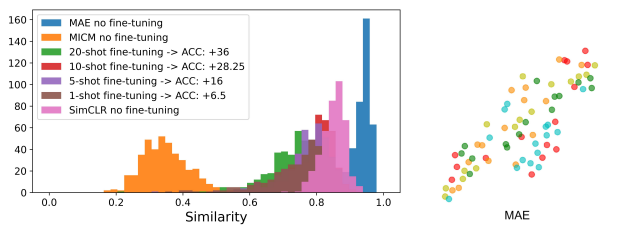


Figure 8: Using the same configuration as in Figure 3, fine-tuning the MAE-trained models on downstream classification tasks.

B MODEL ROBUSTNESS

B.1 Additional downstream tasks

We evaluated MICM on additional downstream tasks, specifically fine-tuning a model trained on miniImageNet for fine-grained visual classification (FGVC) on the CUB dataset, and conducting 5-way 1-shot few-shot open-set recognition tasks (FSOR) on miniImageNet. The results are shown in Table 7:

Table 7: Fine-grained visual classification (FGVC) and few-shot open-set recognition (FSOR) results of three models.

| Method | FGVC (ACC) | FSOR (AUROC) |
|-------------|--------------|--------------|
| MAE | 21.92 | 53.25 |
| SimCLR | 20.27 | 59.92 |
| MICM | 52.93 | 71.12 |

B.2 Further Cross-Domain Few-Shot Comparing

In addition, cross-domain experiments were conducted on the CUB dataset [49], characterized by a relatively minor domain gap. Adhering to the protocols of Poulakakis et al. [35], we trained MICM on the miniImageNet and evaluated it on the CUB dataset’s test set for both 5-way 1-shot and 5-way 5-shot classification tasks. We present the performance results of our MICM model compared to existing unsupervised methods.

As reported in Table 8, our model not only surpasses existing unsupervised methods but also achieves a significant improvement of 4 / 4.3 points over the SOTA Transductive U-FSL method BECLR [35] in 1-shot and 5-shot tasks, respectively.

Table 8: Accuracies (in % \pm std) on miniImageNet \rightarrow CUB. The results of the existing model are cited from BECLR [35]

| Method | miniImageNet \rightarrow CUB | |
|-------------------------|----------------------------------|----------------------------------|
| | 5-way 1-shot | 5-way 5-shot |
| Meta-GMVAE [31] | 38.04 \pm 0.47 | 55.65 \pm 0.42 |
| SimCLR [10] | 38.25 \pm 0.49 | 55.89 \pm 0.46 |
| MoCo v2 [25] | 39.29 \pm 0.47 | 56.49 \pm 0.44 |
| BYOL [22] | 40.63 \pm 0.46 | 56.92 \pm 0.43 |
| SwAV [7] | 38.34 \pm 0.51 | 53.94 \pm 0.43 |
| NNCLR [21] | 39.37 \pm 0.53 | 54.78 \pm 0.42 |
| Barlow Twins [54] | 40.46 \pm 0.47 | 57.16 \pm 0.42 |
| Laplacian Eigenmaps [9] | 41.08 \pm 0.48 | 58.86 \pm 0.45 |
| HMS [53] | 40.75 | 58.32 |
| PsCo [29] | - | 57.38 \pm 0.44 |
| BECLR [35] | 43.45 \pm 0.50 | 59.51 \pm 0.46 |
| MICM (OURS) | 47.44\pm0.65 | 63.86\pm0.42 |

B.3 Sample Bias

Sample bias is an important factor that influences few-shot learning. To evaluate the robustness of our method against sample bias, we investigate two strategies for its mitigation: 1) augmenting the number of support samples, and 2) refining the class prototype using an increased number of query samples (Here, we choose to refine the class prototype using the OpTA algorithm [35]). To

assess the effectiveness of these strategies, we analyze performance variations of both our model and the baseline across different N-way, K-shot, Q-query configurations. This analysis involves, as illustrated in Figure 9, incrementally increasing 1) the number of support samples (K) and 2) the number of query samples (Q). From these experiments, a clear trend emerges: as the count of support or query samples rises – effectively reducing sample bias – the superiority of our model over the baseline becomes increasingly evident. This observation underscores the enhanced adaptability of our approach, especially in scenarios characterized by smaller sample bias, where our model demonstrates a more substantial performance improvement compared to the baseline.

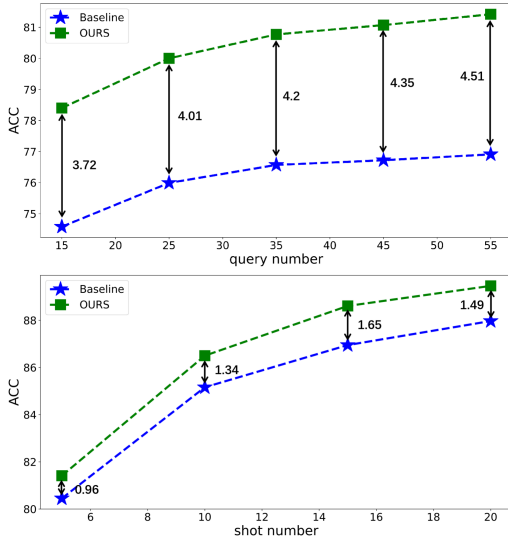


Figure 9: Performance comparison for varying numbers of shots and queries.

C MICM+

We further developed a hybrid method, MICM+, by integrating pseudo-label learning [35] with the transductive OpTA FSL technique [35]. This approach exploits the synergistic potentials of both methods to enhance performance in scenarios with limited labeled data.

C.1 Pseudo Label Training

BECLR’s Pseudo Label Training Stage. The SOTA BECLR [35] utilizes a memory bank alongside clustering techniques to facilitate pseudo-label training. Despite its effectiveness, this method faces challenges such as increased storage requirements and slow convergence rates, stemming from continuous updates between the memory bank and current samples during training.

In our architecture, we experimented with integrating BECLR’s pseudo-label training either from scratch or into a pre-trained MICM model. Our findings, detailed in Table 9, reveal that starting from scratch prolongs training times and diminishes performance, as does introducing pseudo-labeling to a pre-trained model. To address these issues, we propose a novel pseudo-label training strategy using BCE loss, as shown in Figure 10. This method avoids

Table 9: Our MICM model’s inductive few-shot performance on the MiniImageNet dataset after incorporating two pseudo-label training methods.

| Method | Training time | 5-way 1-shot | 5-way 5-shot |
|-----------------------------|--------------------|--------------|--------------|
| MICM | 31.25 Hours | 61.37±0.62 | 81.68±0.43 |
| MICM + BECLR (From scratch) | 46.25 Hours | 57.43±0.62 | 77.34±0.51 |
| MICM + BECLR (A new stage) | 31.25 + 1.50 Hours | 61.30±0.59 | 81.65±0.37 |
| MICM + Pseudo (A new stage) | 31.25 + 0.16 Hours | 66.69±0.65 | 84.03±0.45 |

additional storage costs and can be seamlessly added to existing pre-trained models.

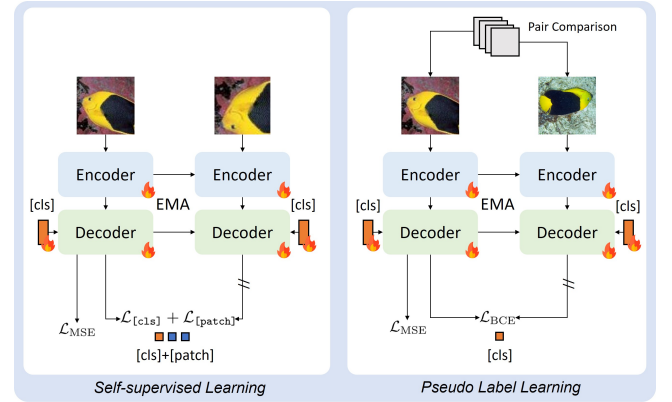


Figure 10: Our pseudo label training stage: further refines samples representations using pair comparison techniques, thereby enhancing the model’s ability to differentiate between various image representations.

Our Pseudo Label Training Stage. Building upon the robust representations developed during the self-supervised learning stage, our primary objective is to enhance the inter-class distinction. To achieve this, we have incorporated a pseudo-label learning method aimed at increasing intra-class compactness. This approach is detailed in Figure 10 and employs a pairwise objective to promote similarity between instance pairs, ensuring effective clustering of instances within the same class.

Pseudo-labels are generated by calculating the cosine distances among all pairs of feature representations, $Z_{[cls]}$, within a mini-batch. These distances are ranked, and each instance is assigned a pseudo-label based on its closest neighbor. Pseudo-labels are thus generated from the most confidently paired positive instances in the mini-batch. Given a mini-batch, S , containing B instances with their features $Z_{[cls]}$, we denote the subset of closest pairs as S' . The pairwise objective is defined using a binary cross-entropy loss (BCE) as follows:

$$\mathcal{L}_{BCE} = \frac{1}{B} \sum_{i=1}^B -\log(\langle \sigma(Z_{[cls]}^{(i)}), \sigma(Z'_{[cls]}^{(i)}) \rangle) \quad (4)$$

where σ is a normalization function applied to each feature vector in S and S' .

In addition to the BCE loss, we continue to use the mean squared error (MSE) loss, \mathcal{L}_{MSE} , from the self-supervised stage to maintain a balance between classification efficacy and model generalization.

Furthermore, we have opted to remove the patch-level loss, $\mathcal{L}_{[\text{patch}]}$, for two primary reasons: Firstly, our pseudo-label training does not involve comparing two views of the same image, making patch-level alignment infeasible. Secondly, maintaining two views and computing patch loss would significantly increase storage demands, necessitating a reduction in batch size. Larger batch size is essential for effective pseudo-label training. This modification, as documented in Table 10, involved reducing the batch size from 128 to 80, leading to a degradation in model performance.

Table 10: MICM+’s transductive few-shot performance after pseudo-label training with/without $\mathcal{L}_{[\text{patch}]}$. When $\mathcal{L}_{[\text{patch}]}$ is retained, a smaller batch size is required due to the increased GPU memory consumption.

| Method | 5-way 1-shot | 5-way 5-shot |
|---------------------|-------------------|-------------------|
| MICM+ w/ Patch loss | 77.96±0.65 | 85.46±0.41 |
| MICM+ | 81.05±0.58 | 87.95±0.34 |

C.2 Optimal Transport-based Distribution Alignment (OpTA)

In line with BECLR’s task setting [35], we employ the OpTA algorithm for transductive few-shot classification tasks. The OpTA process is expressed as follows:

Let $\mathcal{T} = \mathcal{S} \cup \mathcal{Q}$ be a downstream few-shot task. We first extract the support $Z^{\mathcal{S}}$ (of size $NK \times d$) and query $Z^{\mathcal{Q}}$ (of size $NQ \times d$) embeddings and calculate the support set prototypes $P^{\mathcal{S}}$ (class averages of size $N \times d$). Firstly, an optimal transport problem is defined from $Z^{\mathcal{Q}}$ to $P^{\mathcal{S}}$ as:

$$\Pi(r, c) = \left\{ \pi \in \mathbb{R}_+^{NQ \times N} \mid \pi \mathbf{1}_N = r, \pi^T \mathbf{1}_{NQ} = c, r = \mathbf{1} \cdot 1/NQ, c = \mathbf{1} \cdot 1/N \right\} \quad (5)$$

To find a transport plan π (out of Π) mapping $Z^{\mathcal{Q}}$ to $P^{\mathcal{S}}$. Here, $r \in \mathbb{R}^{NQ}$ denotes the distribution of batch embeddings $[z_i]_{i=1}^{NQ}$, $c \in \mathbb{R}^N$ is the distribution of prototypes $[P_i]_{i=1}^N$. The last two conditions in Eq. 2 enforce equipartitioning (i.e., uniform assignment) of Z into the P partitions. Obtaining the optimal transport plan, $\hat{\pi}^*$, can then be formulated as:

$$\pi^* = \underset{\pi \in \Pi(r, c)}{\operatorname{argmin}} \langle \pi, D \rangle_F - \varepsilon \mathbb{H}(\pi), \quad (6)$$

and solved using the Sinkhorn-Knopp [18] algorithm. Here, D is a pairwise distance matrix between the elements of $Z^{\mathcal{Q}}$ and $P^{\mathcal{S}}$ (of size $NQ \times N$), $\langle \cdot, \cdot \rangle_F$ denotes the Frobenius dot product, ε is a regularisation term, and $\mathbb{H}(\cdot)$ is the Shannon entropy.

After Obtaining the optimal transport plan $\hat{\pi}^*$, we use $\hat{\pi}^*$ to map the support set prototypes onto the region occupied by the query embeddings to get the transported support prototypes $\hat{P}^{\mathcal{S}}$ as:

$$\hat{P}^{\mathcal{S}} = \hat{\pi}^{*T} Z^{\mathcal{Q}}, \quad \hat{\pi}_{i,j}^* = \frac{\pi_{i,j}^*}{\sum_j \pi_{i,j}^*}, \forall i \in [NQ], j \in [N], \quad (7)$$

and a comprehensive description of this algorithm is provided in BECLR [35]. Our application of MICM+ with OpTA has led to improved transductive few-shot performance, discussed in subsequent sections.

D ABLATION STUDY

The proposed MICM+ model integrates five key components including: OpTA [35], MICM, (\mathcal{L}_{MSE}), (\mathcal{L}_{CL}) and pseudo-label learning (pseudo). As detailed in Table 11, the baseline model employing OpTA for transductive classification tasks exhibits a notable improvement of 13.6% and 3.5% over traditional inductive classification approaches. This marked enhancement, especially in the 1-shot scenario, can be attributed to OpTA’s effective mitigation of sample bias. Our model MICM combines the \mathcal{L}_{CL} from CL and the \mathcal{L}_{MSE} from MIM, but in the ablation experiments, we separate these two loss functions. It can be observed that the model using only \mathcal{L}_{MSE} has no classification ability, while the model using only \mathcal{L}_{CL} shows relatively good classification performance. However, by combining \mathcal{L}_{MSE} and \mathcal{L}_{CL} , the model’s performance improves by approximately 2.7 / 1.9 points. This result highlights the importance of utilizing generalized features learned during the image reconstruction process. Integration of pseudo-label training contributes additional gains of 2.5% and 1.0% in the 1-shot and 5-shot setups. This enhancement, facilitated by pseudo, further elevate the representational capabilities of features from the pre-training stage and their adaptability to small sample data in downstream tasks.

Table 11: Ablating main components of MICM.

| OpTA | MICM | \mathcal{L}_{MSE} | \mathcal{L}_{CL} | Pseudo | 5-way 1-shot | 5-way 5-shot |
|------|------|----------------------------|---------------------------|--------|---------------------|---------------------|
| - | - | - | - | - | 60.93 ± 0.61 | 80.38 ± 0.34 |
| ✓ | - | - | - | - | 74.58 ± 0.66 | 83.95 ± 0.34 |
| ✓ | ✓ | ✓ | - | - | 26.81 ± 0.43 | 32.94 ± 0.47 |
| ✓ | ✓ | - | ✓ | - | 75.73 ± 0.64 | 85.06 ± 0.35 |
| ✓ | ✓ | ✓ | ✓ | - | 78.40 ± 0.61 | 86.90 ± 0.30 |
| ✓ | ✓ | ✓ | ✓ | ✓ | 81.05 ± 0.58 | 87.95 ± 0.34 |

E COMPUTATIONAL AND STORAGE OVERHEAD

MICM only slightly increases storage and computational and storage overhead compared to iBOT [59], as shown in Tabel 12.

Table 12: Computational and storage overhead of MICM.

| Method | Parameter | FLOAPs | Traing Time | Inference Time |
|--------|-----------|----------|-----------------|---------------------|
| iBOT | 43 M | 691.84 G | 280 (sec/epoch) | 0.121 (sec/episode) |
| MICM | 43 M | 690.71 G | 292 (sec/epoch) | 0.120 (sec/episode) |